Interference effects on the H(2p) to H(2s) branching ratio in the photodissociation of hydrogen and deuterium

J. Alberto Beswick
Laboratoire pour l'Utilisation du Rayonnement Electromagnétique, Université de Paris-Sud, Orsay 91405, France

M. Glass-Maujean
Laboratoire de Spectroscopie Hertzienne de l'Ecole Normale Supérieure, Université Pierre et Marie Curie, Paris 75252, Cédex 05, France

(Received 31 October 1986)

Photodissociation cross sections for both H_2 and D_2 above the H($n=1$)+H($n=2$) threshold are presented. The partial cross sections into H(1s)+H(2s) and H(1s)+H(2p), obtained by full numerical integration of coupled Schrödinger equations, show pronounced oscillations as a function of the excitation energy. These oscillations are the result of a quantum interference effect between two dissociation paths leading to the same final state. The condition for this interference to occur is the existence in the Franck-Condon region of two dissociative states (B and B' in the case considered in this work) which can be excited at the same energy and which are coupled to each other by some nonadiabatic or other electronic interactions. The relationship between the full numerical calculation and the "half-collision" approximation is analyzed in detail. In addition, the predissociation of the D state, which occurs in the same spectral region, has also been studied. The line shapes obtained by solving the appropriate coupled Schrödinger equations are compared with those calculated by the use of perturbation theory. It is shown that, in order to have good agreement with the exact results, it is important to take into account contributions which are usually neglected, namely the contributions from the discrete spectrum of the final dissociative channel. Finally, the branching ratio $\Omega=\sigma(H_2\rightarrow H(1s)+H(2p))/\sigma(H_2\rightarrow H(1s)+H(2s))$ in the case of predissociation has been calculated and compared with other published calculations.

I. INTRODUCTION

The hydrogen molecule provides an ideal test case for the theory of photofragmentation. Since the potential energy curves,[1–4] adiabatic corrections,[5–8] electronic couplings,[9] and transition dipole moments[10–12] are well known, accurate calculations of photodissociation cross sections,[13] line shapes,[14–16] electronic branching ratios,[9,17] angular distributions,[18] as well as polarization of the photofragments fluorescence,[19] can be performed and compared to experiments. With the development of synchrotron radiation sources and vacuum uv (vuv) lasers, it is now becoming possible to measure those quantities in great detail.[20–24]

Although many experiments and calculations have been conducted for H_2, there are still several questions which remain open. Consider, for example, the photon excitation in the range around 14.5 eV ($\lambda\sim 845$ Å). In Fig. 1 the relevant potential energy curves, as calculated by Kołos *et al.*,[1–4] are represented. If the molecule is initially in its ground state, several excited electronic states can be populated through electric dipole transitions which lead to dissociation of H_2 into H(1s)+H(2s,2p) fragments: B, B', C, and D.

The B, B', and C states dissociate directly while the D states, which is bound in this energy region, predissociates through Coriolis coupling to the B' state. Interference between direct dissociation into the B' continuum and

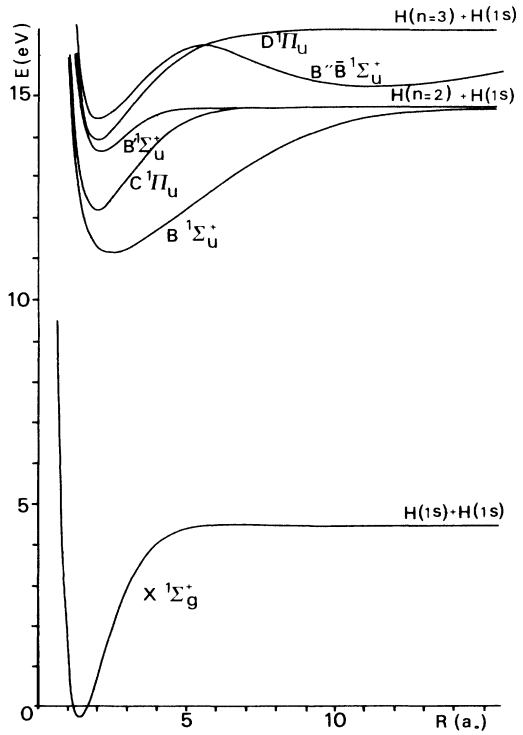

FIG. 1. Relevant potential energy curves for the lowest singlet states of H_2 from Refs. 1–4.

 ©1987 The American Physical Society

predissociation of the D state leads to a unique example of Fano-Beutler resonance line shapes in molecular dissociation.[20] Detailed studies of the linewidth, line shift, and asymmetry parameter of those resonances are important by themselves in order to test the applicability of perturbation theory in the continuum. In addition to the coupling between the D and B' states, the B and B' states are coupled by the radial nonadiabatic interaction (d/dR) at large internuclear distances $(\sim 15a_0)$.[9,17] One may wonder whether this coupling affects the photodissociation cross sections and the absorption line shapes.

It is well know that the branching ratio

$$\Omega=\sigma(H_2\rightarrow H(1s)+H(2p))/\sigma(H_2\rightarrow H(1s)+H(2s)) ,$$

of the fragments is strongly modified by the nonadiabatic coupling between the B and B' states.[9,17,25,26] In the adiabatic approximation the B' state is correlated to $H(2s)+H(1s)$ fragments while the B state correlates to $H(2p)+H(1s)$ fragments. As the D state is coupled to the B' state, its predissociation should produce only $H(2s)$ fragments if the adiabatic correlation applies. The predicted value for Ω would then be zero in contradiction with the measured value of 0.75.[25] In the energy regions between resonances, where only direct photodissociation exists, the two continua B and B' are populated. We show in this paper that in this case new interference effects occur which lead to drastic changes in the branching ratio Ω. It is suggested that these effects can eventually be seen in experiments.

Another interesting question concerns polarization of the Lyman-α fluorescence from the fragments, i.e., the transition $H(2p)\xrightarrow{h\nu'}H(1s)$ of the excited H fragments. In this case one has to consider in addition to the B and B' states the C state which also correlates to $H(2p)$ fragments. In this paper we shall concentrate on the photodissociation cross sections, the calculation of fluorescence polarization will be presented elsewhere.[19(d)]

We have utilized the "artificial channel" method developed by Shapiro,[27] to obtain the photodissociation cross sections and branching ratios. The problem is written in terms of coupled channel Schrödinger equations which are solved by standard scattering techniques. Since the latter are usually designed for second-order differential equations without first-order derivatives, we have used Smith's rotation[28] in order to transform the nonadiabatic couplings between B and B' into potential couplings between "diabatic" $\tilde{B}$ and $\tilde{B}'$ states. Calculations were performed for both H_2 and D_2.

The paper is organized as follows. In Sec. II we present the general equations and the methodology. In Sec. III the results for photodissociation of H_2 and D_2 in the 845–820-Å excitation region are presented and discussed. Finally, Sec. IV is devoted to the conclusions, comparison with the existing measurements, as well as a discussion of some further experiments to test our predictions.

II. GENERAL THEORY

We consider a general one-photon dissociation process from an initial bound state $|\psi_i\rangle$ with energy E_i to a set of final linear independent continuum states $|\psi_{fE}\rangle$ with total energy E. For low-intensity fields, the partial dissociation cross section into channel f for a photon energy $\hbar\omega$ is given by

$$\sigma_{i\rightarrow f}(\hbar\omega)=\frac{4\pi^2(\hbar\omega)}{\hbar c}\,|\langle\psi_i|\boldsymbol{\mu}\cdot\mathbf{e}|\psi_{fE}\rangle|^2,\quad E=E_i+\hbar\omega \tag{1}$$

where $\boldsymbol{\mu}$ is the electronic dipole moment and $\mathbf{e}$ the light polarization vector. In writing Eq. (1) we have assumed that the continuum wave function $|\psi_{fE}\rangle$ is energy normalized. We shall now specify the wave functions further. Here, Hund's case (b) wave functions are appropriate. We thus have quantum numbers N, Λ, and M corresponding to the total angular momentum without the spin ($\mathbf{N}=\mathbf{J}-\mathbf{S}$), its projection onto the internuclear axis and projection onto the laboratory Z axis, respectively. For H_2 the initial state has $\Lambda_i=0$ and $S=0$. In usual experimental conditions all initial M'' sublevels of the initial levels are equally probable, and if we are not interested in angular distribution we sum over all final N' and M' final states. We thus have for linearly polarized light

$$\sigma_{iv''N''\rightarrow f\Lambda'E}=\sum_{N'}\sigma_{iv''N''\rightarrow f\Lambda'N'E} ,$$
$$\sigma_{iv''N''\rightarrow f\Lambda'N'E}=\frac{4\pi^2(\hbar\omega)}{\hbar c}g_{\Lambda'}\frac{(2N'+1)}{3}\begin{pmatrix} N' & 1 & N'' \\ -\Lambda' & \Lambda' & 0\end{pmatrix}|\langle\chi_{iv''N''}|\mu_{\Lambda'}|\chi_{fEN'}\rangle|^2 , \tag{2}$$

where $g_{\Lambda'}=1$ for a Σ final state and 2 otherwise. In Eq. (2) $\mu_{\Lambda'}(R)$ is the Λ' tensorial component of the transition dipole moment (i.e., $\Lambda'=0$ and for a Σ-Σ transition and $\Lambda'=1$ for a Π-Σ transition), $\chi_{iv''N''}(R)$ is the bound vibrational wave function for the initial state and $\chi_{fEN'}(R)$ is the continuum wave function for the final dissociative state f with total energy E and angular momentum N'. For a finite temperature T, the partial photodissociation cross section into channel f is the Boltzmann sum of Eq. (2) over the initial distribution of v'' and N''. Finally, the total photodissociation cross section will be the sum over all final electronic open channels f.

Two different methods have been used recently to calculate the matrix elements of the transition moment between an initial bound and final coupled dissociative wave functions. One can, for example, calculate independently the bound wave functions and solve the coupled equations for the continuum with the appropriate boundary condi-

tions. The matrix elements are then calculated by direct integration. The integrator used for solving the coupled equations needs to provide explicitly the continuum wave functions.[29–31] Another alternative procedure, developed by Shapiro,[27] consists in solving simultaneously a set of coupled equations including the initial and the final states together with an artificial open channel which simulates a feeding channel. With this method the wave functions do not need to be calculated explicitly and the boundary conditions are automatically fulfilled. For details of the method see Ref. 32.

Actually, all these methods are usually designed to handle coupled channel equations in which the couplings are all given by potential functions. When nonadiabatic couplings of d/dR type have to be considered, it is necessary to perform a transformation to a new basis set in which those couplings become potential-like. This is the case for the coupling between the B and B' states in H_2 (see Fig. 2). Defining

$$\tau^{(1)}_{ff'}(R)=-\tau^{(1)}_{f'f}(R)=\left\langle \phi_f \left| \frac{d\phi_{f'}}{dR} \right\rangle \right. ,$$
$$\tau^{(2)}_{ff'}(R)=\left\langle \phi_f \left| \frac{d^2\phi_{f'}}{dR^2} \right\rangle \right. , \tag{3}$$

where the ϕ are adiabatic electronic wave functions, the transformation which is required is such that[28]

$$\frac{d\underline{M}}{dR}=\underline{M}\,\underline{\tau}^{(1)} . \tag{4}$$

If the coupled equations in the adiabatic basis set were

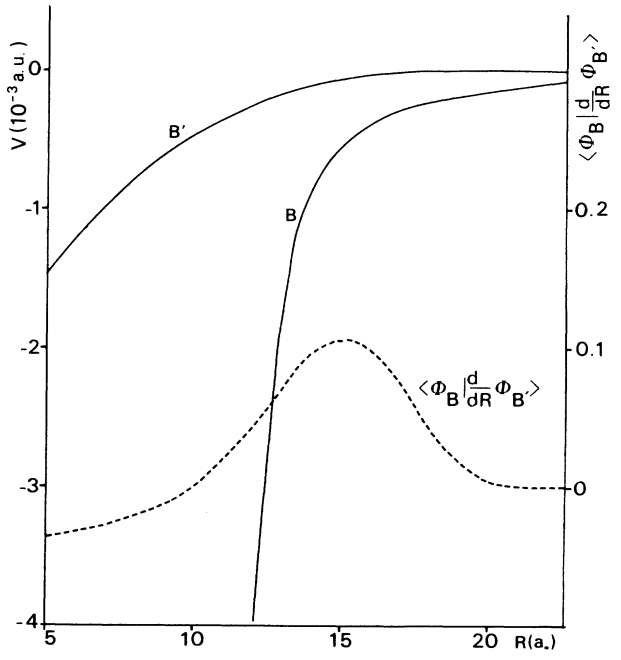

FIG. 2. Asymptotic behavior of the B and B' potential energy curves (from Refs. 1 and 3) and nonadiabatic coupling (in a.u.) from Ref. 9.

$$\left[-\frac{\hbar^2}{2\mu}\frac{d^2}{dR^2}+V(R)-\frac{\hbar^2}{2\mu}\underline{\tau}^{(2)}-\frac{\hbar^2}{\mu}\underline{\tau}^{(1)}\frac{d}{dR}-E \right]\underset{\sim}{\chi}(R)=0 , \tag{5}$$

then in the new basis

$$\underset{\sim}{\bar{\chi}}=\underline{M}\underset{\sim}{\chi} \tag{6}$$

the coupled equations become [using (4)]

$$\left[-\frac{\hbar^2}{2\mu}\frac{d^2}{dR^2}+\underline{M}\,\underline{V}\,\underline{M}^{-1} - \frac{\hbar^2}{2\mu}\underline{M}\left[\underline{\tau}^{(2)}-\frac{d\underline{\tau}^{(1)}}{dR}-(\underline{\tau}^{(1)})^2 \right]\underline{M}^{-1}-E \right]\underset{\sim}{\bar{\chi}}=0 , \tag{7}$$

and the first derivative operator has been eliminated. In order to find $\underline{M}$, Eq. (4) has to be solved. Since it is a first-order differential equation, the solution is determined up to a constant matrix which can be fixed by choosing one point R^* where the two bases, adiabatic and diabatic, are made identical. In the calculations presented in this work this point has been chosen far in the asymptotic region. Thus, the two bases are the same at $R\rightarrow\infty$.

Two approximations have been implemented in our calculations. First, only the B and B' states have been considered to be coupled by nonadiabatic interaction, while the B'' state has been decoupled (see Fig. 1). This is reasonable for energies just above the threshold like those considered here since the B'' channel state is energetically closed and lies well above. For a two-state case, the matrix $\underline{M}$ is

$$\underline{M}=\begin{bmatrix} \cos[\gamma(R)] & \sin[\gamma(R)] \\ -\sin[\gamma(R)] & \cos[\gamma(R)] \end{bmatrix} \tag{8}$$

and integration of Eq. (4) with the condition that the two bases being equal at $R\rightarrow\infty$, gives

$$\gamma(R)=\int_R^{\infty}\tau^{(1)}_{21}(R')dR'=\int_{\infty}^{R}\tau^{(1)}_{12}(R')dR' . \tag{9}$$

Secondly, we have neglected the terms in parentheses in Eq. (7). Estimation of their contribution yields in our case very small corrections. Notice that if the closure relation is used:

$$\underline{\tau}^{(2)}=\frac{d\underline{\tau}^{(1)}}{dR}+(\underline{\tau}^{(1)})^2 , \tag{10}$$

the term in parentheses in Eq. (7) vanishes identically. Thus, our approximation is consistent with the fact that we have neglected all nonadiabatic couplings with other states.

With the approximation above, the coupled equations for the B and B' states become

$$\left[-\frac{\hbar^2}{2\mu}\frac{d^2}{dR^2}+(V_1\cos^2\gamma+V_2\sin^2\gamma)-E\right]\bar{\chi}_1 = -[(V_2-V_1)\sin\gamma\cos\gamma]\bar{\chi}_2 , \quad (11)$$

$$\left[-\frac{\hbar^2}{2\mu}\frac{d^2}{dR^2}+(V_1\sin^2\gamma+V_2\cos^2\gamma)-E\right]\bar{\chi}_2 = -[(V_2-V_1)\sin\gamma\cos\gamma]\bar{\chi}_1 .$$

In addition to the B and B' states, two other excited states have to be considered in the same energy region. These are the C and D states. For the energies considered here the C state is excited above its dissociation limit while the D state is excited below its own dissociation limit. However, the Π^+ component of the D state can be coupled by nonadiabatic interactions to the lower-lying states and undergo predissociation. Inspection of different couplings reveals that the $D(\Pi^+)$ state is coupled efficiently only to the B' state by Coriolis coupling. This can be seen as follows. Since D is a Π state, radial nonadiabatic coupling will only exist between D and C states ($\Delta\Lambda=0$), while Coriolis coupling will exist between $D(\Pi^+)$ and both B and B' states ($\Delta\Lambda=\pm1$). Inspection of Fig. 1 shows that only the B' state lies close enough in energy to the D state to have non-negligible vibrational wave function overlap. In addition, there is an electronic propensity rule. The D state can be approximately described by a $3p\pi$ orbital. On the other hand, the B and B' states can be described by $2p\sigma$ and $3p\sigma$ orbitals, respectively. Therefore, only the $D(\Pi^+)$ and B' states will be coupled by the Coriolis interaction at this level of approximation. These conclusions have been born out by the measurements on the predissociation lifetimes of the $D(\Pi^-)$ levels[23,33] which are only coupled to the C continuum. The results show clearly that this coupling is very weak and thus, it can be neglected for both Π^+ and Π^- components.

There are still two other interactions which have not been considered yet. These are the Coriolis coupling between C and the B and B' states, and the radial nonadiabatic coupling between the B and B' states. The former can only be efficient between the C and B states, both from electronic configuration and overlap reasons, while the latter will be important at large internuclear distances where the B and B' states come close together. In our calculations we have checked that the Coriolis coupling between the C and B states has a negligible effect on the results. On the other hand, the radial nonadiabatic couplings between the B and B' states at large internuclear distances has a pronounced effect on the final states of the fragments.

Therefore, the calculations presented in this paper include the ground state X and the four excited states B, B', C, and D potential energy curves[1-4] and their adiabatic corrections,[5-8] the transition dipole moments between X and the B, B', C, and D states,[10-12] and the two most important couplings discussed above, namely, the Coriolis coupling between the D and B' states,[15] and the radial nonadiabatic coupling between the B and B' states.[9]

Concerning the Coriolis coupling,

$$\langle\Lambda\,|\,H_c\,|\,\Lambda\pm1\rangle = -\frac{\hbar^2}{2\mu R^2}\sqrt{L(L+1)-\Lambda(\Lambda\pm1)}\times\sqrt{N(N+1)-\Lambda(\Lambda\pm1)} , \quad (12)$$

where we have assumed that the electronic orbital angular momentum L is meaningful. This is a reasonable approximation for a Rydberg state in H_2. The D state is predominantly $3p\pi$ ($L=1$) and the B' state $3p\sigma$ ($L=1$). Thus, we have for the $|\,^1\Pi^+\rangle=(2)^{-1/2}(\,|\,\Lambda=1\rangle+|\,\Lambda=-1\rangle)$ parity component

$$\langle D\,^1\Pi^+\,|\,H_c\,|\,B'\,^1\Sigma\rangle = -\frac{\hbar^2}{\mu R^2}\sqrt{N(N+1)} , \quad (13)$$

and 0 for the $D\,^1\Pi^-$.

We notice at this point that the C state is uncoupled from the others and can thus be studied separately. Its contribution will be important, however, in a following paper when polarization of the fluorescence from the fragments will be considered.[19d].

The integrator used in the artifical channel code is the "amplitude density" algorithm developed by Johnson and Secrest.[34] The integration was performed from 0.4 to 35.0 a.u. with 8000 steps. The potentials were interpolated between the *ab initio* points with a natural spline fitting.[35]

III. RESULTS AND DISCUSSION

A. Direct dissociation of H_2

It is particularly interesting to discuss the $P(1)$ transitions ($N''=1\rightarrow N'=0$) which do not exhibit resonance peaks (the D levels cannot be excited since $N'=0$ does not exist for a Π state). For the $P(1)$ transition the effect of the radial nonadiabatic coupling between the B and B' states can thus be easily analyzed.

In Fig. 3 we present the photodissociation spectrum for

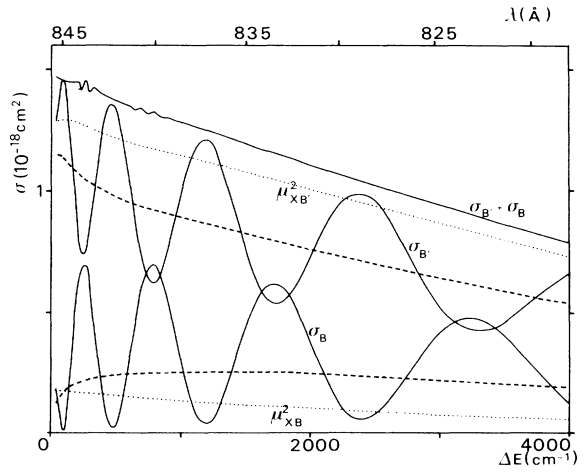

FIG. 3. Partial and total photodissociation cross sections in the excitation range corresponding to 40–4000 cm^{-1} of excess energy for the $P(1)$ transition. The solid lines correspond to the full calculation. The dotted lines correspond to a simple Born-Oppenheimer approach without any coupling. The dashed lines are the results obtained from the excitation of the single B' state and taking into account the coupling with B (see text).

that particular transition in the excitation range from 845 to 820 Å (corresponding to 40—4000 cm^{-1} of energy above the dissociation threshold). The most remarkable feature is the oscillating behavior of the partial cross sections, the maxima for the channel B' giving H(2s)+H(1s) fragments occurring at the minima for the channel B giving H(2p)+H(1s) fragments. On the other hand, the sum of the two partial cross sections is equal to the sum of the previously calculated cross sections ignoring the coupling between the two channels B and B',[13] except for tiny oscillations ($<2\%$) around the maxima of the H(2p)-to-H(2s) branching ratio (see Fig. 3).

The rationalization of these results is the following. Consider the final state H(2s)+H(1s). There are two paths which both lead to this same final state: path 1, excitation of the B' state by photon absorption and adiabatic dissociation; path 2, excitation of the B state by photon absorption and nonadiabatic transition to the B' state. For the final state H(2p)+H(1s) there are also two paths which are the symmetrical of the above. Since the region of the nonadiabatic transitions is far ($\sim 15a_0$) from the Franck-Condon region ($\sim 1.6a_0$), we can separate to a good approximation the photon excitation from the nonadiabatic transition.

The quantum-mechanism amplitude for dissociation into a particular channel [H(2s)+H(1s), for instance] will then be the sum of the amplitudes through paths 1 and 2 discussed above. Since the photodissociation cross section will be given by the square of this sum, we expect quantum interference effects. This is what is seen in Fig. 3. It is striking that this interference leads to such a dramatic effect on the partial cross section in spite of the fact that in the case considered here the cross section for the B' channel is almost ten times larger than the B cross section if the nonadiabatic coupling is neglected. On the other hand, if both B and B' channels are observed together the interference effect cancels and this is exactly the behavior shown by the sum $\sigma_B+\sigma_{B'}$ (see Fig. 3).

More interestingly perhaps is the results obtained when the transition dipole moment μ_{XB} is neglected, i.e., artificially set to zero. The oscillations in the partial cross sections disappear but it remains an appreciable probability for feeding the B channel. No interference effect can occur in this case since only path 1 remains, but the B channel can still be populated through a nonadiabatic transition.

More precisely, let $\chi_B^{(0)}$ and $\chi_{B'}^{(0)}$ be the vibrational functions, solution of the uncoupled problem at total energy E. In the asymptotic region ($R\to\infty$) these functions behave as

$$\chi_B^{(0)}(R)\underset{R\to\infty}{\sim}\frac{\sin(k_BR+\varphi_B)}{k_B^{1/2}}\ , \tag{14a}$$

$$\chi_{B'}^{(0)}(R)\underset{R\to\infty}{\sim}\frac{\sin(k_{B'}R+\varphi_{B'})}{k_{B'}^{1/2}}\ , \tag{14b}$$

where the proportionality constant is equal to $(2\mu/\pi\hbar^2)^{1/2}$ for energy-normalized wave functions. The wave vectors $k_B=\{2\mu[E-V_B(\infty)]\}^{1/2}/\hbar$ and $k_{B'}=\{2\mu[E-V_{B'}(\infty)]\}^{1/2}/\hbar$ are identical in our calculations since we have taken the two states to be degenerate at infinity. In any case, the arguments which follow are independent of whether the two states are degenerate or not. The important assumption is the following: the nonadiabatic coupling induces transitions between the two states in a region of $R\sim R_*$ very far from the Franck-Condon region. This is exactly the situation in our problem.

With the assumption above we can now write a general solution for the coupled problem. In the region of the Franck-Condon transition we can write the two linearly independent solutions as

$$\begin{aligned}&|\chi_B\rangle=\chi_B^{(0)}(R)\,|B\rangle\ ;\\ &|\chi_{B'}\rangle=\chi_{B'}^{(0)}(R)\,|B'\rangle\ \text{ for } R\ll R_*\ ,\end{aligned} \tag{15}$$

with $\chi_B^{(0)}$ and $\chi_{B'}^{(0)}$ being the solutions of the uncoupled problem.

In the region $R\sim R_*$ we cannot give an analytical exact solution of the coupled problem, but in the asymptotic region two linearly independent solutions would be[36]

$$\begin{aligned}|\chi_B\rangle_{R\to\infty}\sim\ &(1-P)^{1/2}\frac{\sin(k_BR+\delta_B)}{k_B^{1/2}}\,|B\rangle\\ &+P^{1/2}\frac{\sin(k_{B'}R+\delta_B)}{k_{B'}^{1/2}}\,|B'\rangle\ ,\\ |\chi_{B'}\rangle_{R\to\infty}\sim\ &-P^{1/2}\frac{\sin(k_BR+\delta_{B'})}{k_B^{1/2}}\,|B\rangle\\ &+(1-P)^{1/2}\frac{\sin(k_{B'}R+\delta_{B'})}{k_{B'}^{1/2}}\,|B'\rangle\ ,\end{aligned} \tag{16}$$

where P, δ_B, and $\delta_{B'}$ are provided by the integration of the coupled equations in the region of the interaction. Their interpretation is the following: P is the probability to have a transition from one state to the other in a single passage through the interaction region, while δ_B and $\delta_{B'}$ are two phase shifts.

The solutions $|\chi_B\rangle$ and $|\chi_{B'}\rangle$ in Eq. (16) do not have the appropriate boundary asymptotic behavior for photodissociation problems. The wave functions we want are of the form[37]

$$\begin{aligned}|\overline{\chi_B}\rangle_{R\to\infty}\sim\ &\frac{e^{ik_BR}}{k_B^{1/2}}\,|B\rangle+S_{BB}^*\frac{e^{-ik_BR}}{k_B^{1/2}}\,|B\rangle\\ &+S_{BB'}^*\frac{e^{-ik_{B'}R}}{k_{B'}^{1/2}}\,|B'\rangle\ ,\end{aligned} \tag{17a}$$

$$\begin{aligned}|\overline{\chi_{B'}}\rangle_{R\to\infty}\sim\ &\frac{e^{ik_{B'}R}}{k_{B'}^{1/2}}\,|B'\rangle+S_{BB'}^*\frac{e^{-ik_BR}}{k_B^{1/2}}\,|B\rangle\\ &+S_{B'B'}^*\frac{e^{-ik_{B'}R}}{k_{B'}^{1/2}}\,|B'\rangle\ .\end{aligned} \tag{17b}$$

Equation (17a), for example, means that the dissociative H(2p)+H(1s) channel corresponds to a unit flux outgoing $|B\rangle$ wave and a superposition of ingoing $|B\rangle$ and $|B'\rangle$ waves with coefficients related to the usual scattering matrix $\underline{S}$.

We thus need to take linear combinations of Eq. (16) in order to obtain the appropriate functions (17):

$$|\overline{\chi_B}\rangle = |\chi_B\rangle S^H_{BB} + |\chi_{B'}\rangle S^H_{B'B} ,$$
$$|\overline{\chi_{B'}}\rangle = |\chi_B\rangle S^H_{BB'} + |\chi_{B'}\rangle S^H_{B'B'} , \tag{18}$$

where the coefficients of the transformation have been denoted by S^H_{ij} meaning "half-collision S matrix" for reasons which will become clear shortly. Their explicit expressions are [from Eqs. (16), (17), and (18)]

$$S^H_{BB} = (1-P)^{1/2} e^{i\delta_B}, \quad S^H_{B'B} = -P^{1/2} e^{i\delta_{B'}} ,$$
$$S^H_{BB'} = P^{1/2} e^{i\delta_B}, \quad S^H_{B'B'} = (1-P)^{1/2} e^{i\delta_{B'}} , \tag{19}$$

and we also get from this calculation

$$S_{BB} = (1-P) e^{2i\delta_B} + P e^{2i\delta_{B'}} ,$$
$$S_{B'B'} = P e^{2i\delta_B} + (1-P) e^{2i\delta_{B'}} , \tag{20}$$
$$S_{BB'} = S_{B'B} = \sqrt{P(1-P)}\,(e^{2i\delta_B} - e^{2i\delta_{B'}}) .$$

Now the photodissociation cross sections into B and B' channels are given by

$$\sigma_B \propto |\langle \chi_X | \mu | \overline{\chi_B} \rangle|^2 = |\mu_{XB} S^H_{BB} + \mu_{XB'} S^H_{B'B}|^2 ,$$
$$\sigma_{B'} \propto |\langle \chi_X | \mu | \overline{\chi_{B'}} \rangle|^2 = |\mu_{XB} S^H_{BB'} + \mu_{XB'} S^H_{B'B}|^2 , \tag{21}$$

where we have denoted by $\mu_{XB} = \langle \chi_X | \mu | \chi_B \rangle$ and $\mu_{XB'} = \langle \chi_X | \mu | \chi_{B'} \rangle$ the transition matrix elements from the ground state X to the excited states which behave asymptotically as in Eq. (14). But those states are equal to the unperturbed ones in the Franck-Condon region, so that μ_{XB} and $\mu_{XB'}$ are essentially identical to those calculated in the uncoupled problem. Now it is clear why we have denoted by S^H_{ij} the coefficients of the transformation (18). According to (21) the amplitude for photodissociation into channel B is the sum of two amplitudes: one corresponds to excitation of the uncoupled channel B multiplied by the half-collision probability amplitude to stay in that state, while the other corresponds to excitation to the unperturbed B' state multiplied by the probability amplitude to jump to the state B from the B' in the half collision following the photon excitation. This is in agreement with our qualitative description we gave at the beginning of this section.

Using Eqs. (19), we finally get

$$\sigma_{X\to B} \propto \mu^2_{XB}(1-P) + \mu^2_{XB'} P - 2\mu_{XB}\mu_{XB'}\sqrt{P(1-P)}\cos(\delta_B - \delta_{B'}) ,$$
$$\sigma_{X\to B'} \propto \mu^2_{XB} P + \mu^2_{XB'}(1-P) + 2\mu_{XB}\mu_{XB'}\sqrt{P(1-P)}\cos(\delta_B - \delta_{B'}) , \tag{22}$$

and of course $\sigma_B + \sigma_{B'} \propto \mu^2_{XB} + \mu^2_{XB'}$. Equations (22) reproduces exactly the behavior observed in Fig. 3.

The phase difference $(\delta_B - \delta_{B'})$ can be related to the difference between the "local" phases of the unperturbed wave functions at the transition point $R_* \sim 15 a_0$ (see Fig. 4). This difference would be $\varphi_B - \varphi_{B'}$ [Eq. (14)] if the asymptotic forms of the wave functions were reached, which is not fully the case in our problem in particular for the B state (see Figs. 2 and 4).

From Fig. 3, it is possible to obtain approximate values for P at the points where $\cos(\delta_B - \delta_{B'}) = \pm 1$. It is also possible to obtain P in a different way. We have performed calculations by setting artificially $\mu_{XB} = 0$. If this is the case, no interference exists and the cross sections are given by

$$\sigma_{X\to B'} \propto \mu^2_{XB'}(1-P) ,$$
$$\sigma_{X\to B} \propto \mu^2_{XB'} P , \tag{23}$$

from which P can be determined. Both calculations give similar results. The probability P varies smoothly from 0.1 to 0.2 in the energy range between 10 to 500 cm^{-1} above threshold (see Fig. 5).

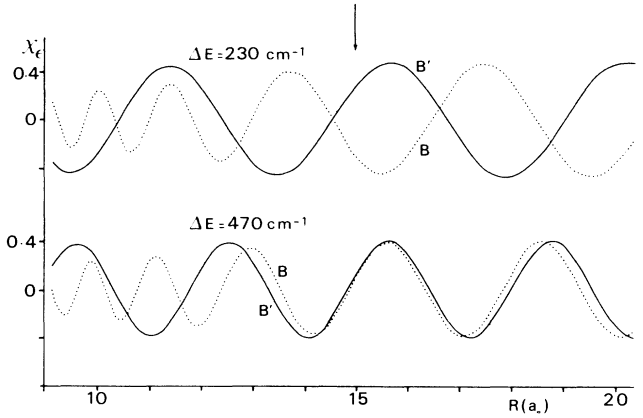

FIG. 4. Unperturbed vibrational wave functions of the B and B' states in the coupling region for two different excess energy values. The vertical arrow indicates the position of the maximum of the nonadiabatic coupling (see Fig. 2). $\Delta E = 230$ cm^{-1} of excess energy corresponds to a minimum of the interference effect between the two channels, while $\Delta E = 470$ cm^{-1} corresponds to a maximum (see Fig. 3).

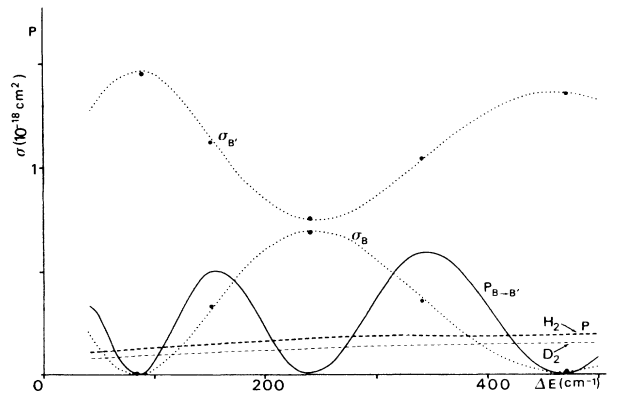

FIG. 5. Partial photodissociation cross sections into the B and B' channels for H_2 (dotted lines) in the 40–500 cm^{-1} excess energy range, single passage transition probability P for H_2 and D_2 (dashed lines), and collisional transition probability $P_{B\to B'}$ for H_2 (solid line). The points are the results of an approximate calculation using the half collision transition probability P (see text). Note that the vertical scale is the same for P and σ in Mb.

A further check of our analysis of the photodissociation cross section can be performed. The probability for a nonadiabatic transition from B to B' to a "full" collision is given by $P_{B\to B'}=|S_{BB'}|^2$. Using (20) we get

$$P_{B\to B'}=4P(1-P)\sin^2(\delta_B-\delta_{B'}) , \tag{24}$$

which, when $\sin^2(\delta_B-\delta_{B'})$ is replaced by its mean value $\frac{1}{2}$, gives the well-known expression $P_{B\to B'}=2P(1-P)$ for the nonadiabatic transition probability in a *full collision* in terms of the probability P to jump from one state to the other in a *single passage*.[36]

In Fig. 5 we have plotted the *full collision* probability $P_{B\to B'}$, as calculated by full numerical integration of the coupled equations, together with the partial photodissociation cross sections into the B and B' channels, in the energy range between 10 and 500 cm^{-1} above threshold. Indeed, the behavior of $P_{B\to B'}$ is in perfect agreement with Eq. (24). For instance, at 240 cm^{-1} there is maximum interference. P is ~ 0.17 at this energy. Substituting that value into Eq. (22) and using μ_{XB} and $\mu_{XB'}$ calculated without couplings we get $\sigma_{B'}=0.752\times10^{-18}$ cm^2 and $\sigma_B=0.692\times10^{-18}$ cm^2. These points are also represented in Fig. 5. The more precise values calculated with the artificial channel method are $\sigma_{B'}=0.747\times10^{-18}$ cm^2 and $\sigma_B=0.691\times10^{-18}$ cm^2, a remarkable agreement.

There is one additional counterintuitive result from Eqs. (22) and (24) which can be noticed in Fig. 5: the points for which there is maximum interference in the photodissociation cross sections correspond in fact to zero probability for the nonadiabatic transition $P_{B\to B'}$ in a single collision.

Finally, it is worth noting that from Eqs. (19) and (20) we can write

$$\underline{S}=(\underline{S}^H)^T(\underline{S}^H) , \tag{25}$$

which relates the full collision $\underline{S}$ matrix to the product of the half collision matrix $\underline{S}^H$ by its transpose.

In Fig. 6 we present the branching ratio

$$\Omega\equiv\sigma(H_2\to H(1s)+H(2p))/\sigma(H_2\to H(1s)+H(2s))$$
$$=\sigma(B)/\sigma(B')$$

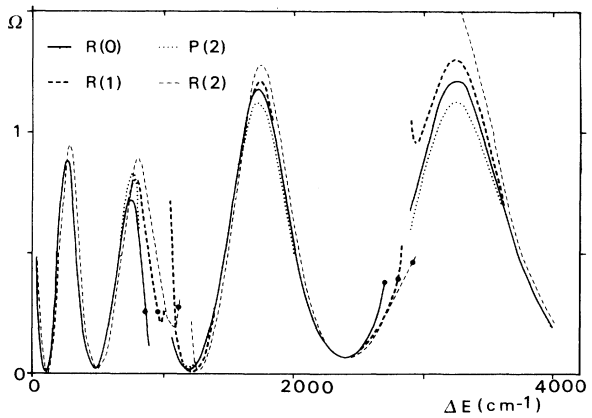

FIG. 6. Branching ratio $\sigma(H_2\to H(1s)+H(2p))/\sigma(H_2\to H(1s)+H(2s))$ as a function of the excess energy for different rotational transitions in H_2. The points represent the Ω values at the maximum of the predissociation peaks.

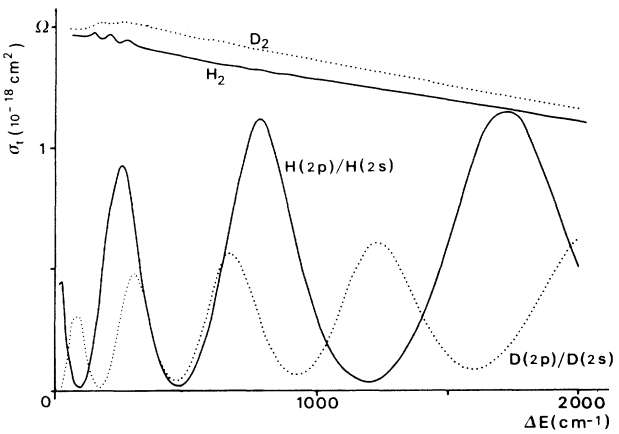

FIG. 7. Comparison between the total photodissociation cross sections and branching ratios $\sigma(H_2\to H(1s)+H(2p))/\sigma(H_2\to H(1s)+H(2s))$ as functions of the excess energy for H_2 (solid line) and D_2 (dotted line). Note that the vertical scale is the same for Ω and σ_T in Mb.

as a function of the excess energy for different rotational transitions. Except in the vicinity of the predissociation peaks discussed below (see Sec. III C), the oscillations are very similar. This is expected since the only difference is the small change in the effective potential for low N.

B. Direct photodissociation in D_2

In Fig. 7 we have plotted the total photodissociation cross sections for the $P(1)$ transition, for both H_2 and D_2 together with the branching ratio $\Omega=\sigma_B/\sigma_{B'}$.

The small difference ($\sim 7\%$) between the total cross sections for H_2 and D_2 at the same final total energy is due only to the difference in spatial extension of the ground vibrational wave function.[38] The same is true for the average value of the branching ratio Ω although in this case the isotope effect is larger (~ 1.8).

There are two other, probably more significant, differ-

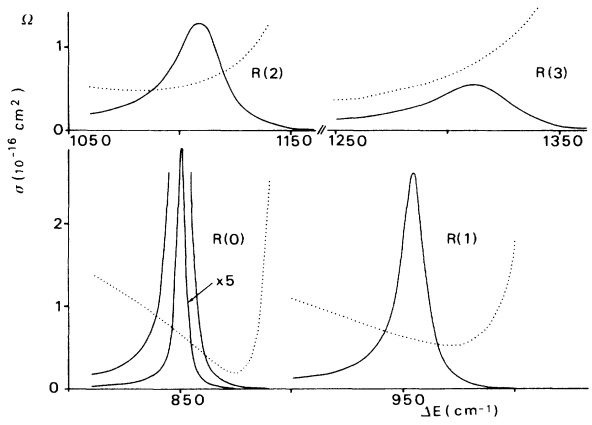

FIG. 8. Predissociation profiles and branching ratios $\sigma(H_2\to H(1s)+H(2p))/\sigma(H_2\to H(1s)+H(2s))$ for different rotational H_2 ($D\leftarrow X$) transitions. Note that the vertical scales are the same for Ω and σ in 10^{-16} cm^2.

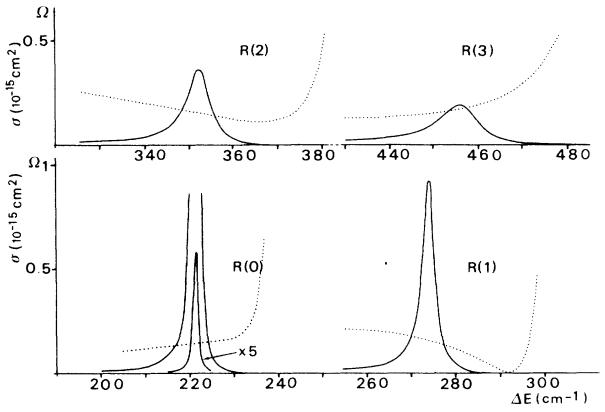

FIG. 9. Same as Fig. 8 for D_2.

ences between the results for H_2 and D_2. The amplitude of the oscillations in the partial cross sections (and therefore in the branching ratio) is smaller in the case of D_2 while the frequency is higher. Qualitatively this can be understood as follows. The frequency of the oscillations depends on the variation of the phases δ_B and $\delta_{B'}$ with energy. This variation is faster for D_2 than for H_2 due to the difference of the reduced masses, as can be easily shown for simple square well potentials. For instance, let us replace the two potentials V_B and $V_{B'}$ by two square wells with ranges R_B and $R_{B'}$, and depths D_B and $D_{B'}$. If the kinetic energy E is much smaller than D_B and $D_{B'}$, the phase difference at the transition point $R_* > R_B$ and $R_{B'}$ will be of the form

$$\delta_B - \delta_{B'} \cong cte + \frac{\sqrt{2\mu E}}{\hbar}(R_{B'} - R_B) \ . \tag{26}$$

We expect, thus, a $\sqrt{\mu E}$ dependence of the frequency of the oscillations. This is already clear for H_2 itself. The positions of maxima and minima of Ω in Fig. 7 follow a $\sqrt{E}$ law. Since $\mu_{D_2} \sim 2\mu_{H_2}$ the frequency of the oscillations for D_2 is roughly $\sqrt{2}$ that of H_2.

The amplitudes, on the other hand, depend on the value of P, the transition probability in a single passage through the critical region R_*. For D_2 this probability is smaller, since the relative velocity of the fragments is slower implying that the passage through the critical region is more "adiabatic." This is seen in Fig. 5 where we have plotted P for both isotopes. Indeed, P_{H_2} is larger than P_{D_2} by a factor of ~ 1.2.

C. Predissociation profiles

One other outcome of our calculations is that we obtain directly the predissociation profiles corresponding to bound levels of the $D(^1\Pi_u^+)$ state (see Figs. 8 and 9). Since direct dissociation and predissociation occur simultaneously in this energy region, Fano-Beutler profiles are seen in the experiments.[39,40] In fact, they were among the first asymmetric absorption profiles observed. Their general form is[41]

$$\sigma(E) = \sigma_0 + \sigma_1(\varepsilon + q)^2/(1+\varepsilon^2) \ , \qquad \varepsilon = 2(E - E_0)/\Gamma \ , \tag{27}$$

where E_0 is the resonance position, Γ the total width, and q the asymmetry parameter of the resonance. We have fitted our calculated profiles to the form given by Eq. (27). The values of Γ and q for a number of profiles are given in Tables I and II, together with the available experimental values.[20] The agreement between the calculated and experimental values is reasonably good, the difference being of the order of 10%. A much better agreement was obtained by Jungen using multichannel quantum-defect theory (MQDT).[16] The reason for this can only come from the inclusion in the MQDT treatment of the interaction with all other Rydberg states, while we have limited our calculations to a subset of the whole manifold of states. It would be interesting in the framework of our treatment, to study this effect by including the B'' and the D' state, for instance, which are probably the states coupled most strongly to D. We are planning to perform this calculation in the future.

Another way of calculating Γ and q is by the use of perturbation theory.[41] Since these parameters are determined by the wave functions in the region of $R \sim 1.5a_0$ where the nonadiabatic couplings may be neglected, and we are interested in the total width, we may work to a very good approximation with the unperturbed wave functions.

TABLE I. Profile parameters Γ (cm^{-1}) and q for the R lines of the $D(v=3) \leftarrow X$ transition in H_2 and $D(v=4) \leftarrow X$ in D_2. Γ_p and q_p refer to the perturbative approach neglecting the modification of the discrete state while Γ_f and q_f are the values from the full calculation. Γ_{expt} and q_{expt} are the experimental values from Ref. 20.

		Γ_p	Γ_f	Γ_{expt}	q_p	q_f	q_{expt}
(H_2)	$J=1$	4.3	4.3		22	21	18±2
$v=3$	$J=2$	13	13	14.5±0.7	11	10.4	9±1
	$J=3$	26	26		7.3	7.6	
	$J=4$	43.5	45		5.5	5.1	
D_2	$J=1$	1.1	1.1		44	39	
$v=4$	$J=2$	3.2	3.3		22	19	
	$J=3$	6.5	6.5		14.5	12.5	
	$J=4$	11	11		11	9	

TABLE II. Same as Table I for the $R(1)$ lines of the D ($v=4$ and 5)$\leftarrow X$ transitions in H_2.

	Γ_p	Γ_f	Γ_{expt}	q_p	q_f	q_{expt}
$v=4$	13.2	13.2	14.5±0.7	10.7	10.1	9±1
$v=5$	13.1	13	13.8±0.9	10.5	9.8	9±1

Neglecting the variation with energy of the discrete-continuum couplings and of the transition dipole moment matrix elements, one obtains[41]

$$\sigma_1=\frac{4\pi^2(\hbar\omega)}{\hbar c}\,|\langle\psi_X\,|\,\boldsymbol{\mu}\cdot\mathbf{e}\,|\,\psi_{B'}\rangle|^2\,, \tag{28}$$

$$\Gamma=2\pi V^2\,, \tag{29}$$

where V is the matrix element between D and B' states of the Coriolis coupling defined in Eq. (12)

$$q=\frac{\langle\psi_D\,|\,\boldsymbol{\mu}\cdot\mathbf{e}\,|\,\psi_X\rangle}{\pi V\langle\psi_{B'}\,|\,\boldsymbol{\mu}\cdot\mathbf{e}\,|\,\psi_X\rangle}\,. \tag{30}$$

We have computed Γ and q, Eqs. (29) and (30), utilizing the Numerov integration technique. The results are presented in Table I. There is perfect agreement between the values calculated by the two methods, perturbation and artificial channel, for the linewidth Γ. It is less so for the asymmetry parameter q and this makes a noticeable effect on the line strength. In Fig. 10 we present the results of both calculations for a particular transition $[3\leftarrow 0,R(1),D\leftarrow X]$ in H_2. In addition to the difference in the calculated line strength there is a small shift (of the order of the linewidth) between the two profiles.

Both effects can be understood by the influence of two factors: (a) the variation of the matrix elements with energy which was neglected above; (b) the couplings to the bound levels of the dissociative state. Both contribute to a modification of the discrete state $|\psi_D\rangle$ to

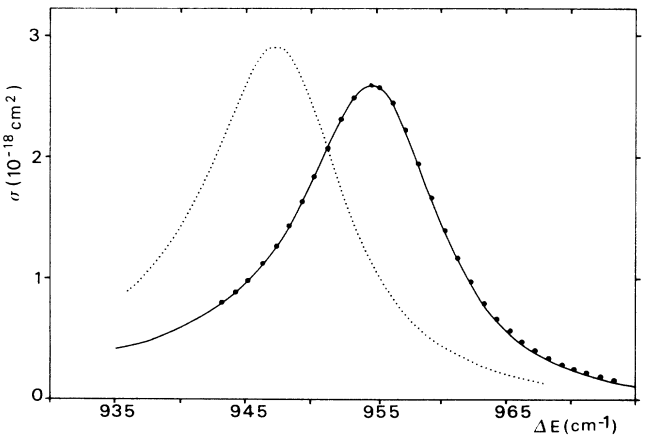

FIG. 10. Calculated predissociation profiles for the $R(1)$, $D\,^1\Pi_u^+$, $v'=3\leftarrow X\,^1\Sigma_g^+$, $v''=0$ transition in H_2. Solid line: full calculation. Dotted line: result of the calculation using the Fano's perturbation approach not including the modification of the discrete state. The solid circles correspond to a similar calculation but take this modification into account.

$$|\bar{\psi}_D^v\rangle=|\psi_D^v\rangle+P\int dE'\frac{V_{E'}}{E_D^v-E'}\,|\psi_{B'}^{E'}\rangle + \sum_{v'}\frac{V_{v'}}{E_D^v-E_{B'}^{v'}}\,|\psi_{B'}^{v'}\rangle\,, \tag{31}$$

where the contribution of the continuum and discrete levels of the B' state are included to first order.

The modified resonance position is

$$\bar{E}_D^v=E_D^v+P\int dE'\frac{|V_{E'}|^2}{E_D^v-E'}+\sum_{v'}\frac{|V_{v'}|^2}{E_D^v-E_{B'}^{v'}}\,, \tag{32}$$

while $\bar{q}$ will be given by Eq. (30) in which ψ_D is replaced by $\bar{\psi}_D$. On the other hand, V in Eqs. (29) and (30) is not modified in this first-order treatment.

When Eqs. (31) and (32) are used the agreement between the two calculations becomes excellent (see Fig. 10). It is interesting to note that the level shift due to the continuum is only 1.0 cm^{-1}, while the contribution of the discrete levels of B' located at 2000 or 3000 cm^{-1} below accounts for the 6.5 cm^{-1} remaining shift. This is due to the fact that although the energy difference between the B' and the D bound levels is large the overlaps of their vibrational wave functions are very favorable.

For the asymmetry parameter q, the effect is very similar. The artificial channel calculated value is -10.4. Perturbation calculation with the unmodified discrete state $|\psi_D^v\rangle$ gives -11.06. The contribution of the continuum term in Eq. (31) still lowers the q value by -0.10 while the discrete contribution raises q by $+0.77$. The final result is -10.39 in very good agreement with the artificial channel value. This comparison stresses the importance of contributions which are usually neglected, namely the existence of a discrete spectrum in dissociative channels.

D. Branching ratio $\sigma(\mathrm{H}(2p))/\sigma(\mathrm{H}(2s))$ in the case of predissociation

When predissociation occurs the B' state is predominantly populated in the small-R region where it is populated directly from the bound levels of the D state by Coriolis coupling. Therefore, in predissociation the situation is very much similar to the case when μ_{XB} was artificially set to zero. We expect a smooth variation of the branching ratio as a function of the initially D bound level excited. Explicitly, we should have for the fraction of H(2s) atoms, according to Eq. (23),

$$\omega\equiv\frac{f(\mathrm{H}(2s))}{f(\mathrm{H}(2s))+f(\mathrm{H}(2p))}\equiv\frac{\sigma_{X\to B'}}{\sigma_{X\to B'}+\sigma_{X\to B}}=1-P\,. \tag{33}$$

Let us turn now to our calculated values. We present in

TABLE III. Fraction of H(2s) atoms produced in the photopredissociation of H_2 and D_2 [$R(1)$ lines of the $D \leftarrow X$ transition]. The first column presents the results from the full calculation. The second column is the approximate value using the half collision transition probability P (see text).

	Calculations			
	$\omega=\frac{\sigma_{B'}}{\sigma_B+\sigma_{B'}}$	$\omega=1-P$	Expt.	Ref.
H_2 ($D,v'=3$) $E=950$ cm^{-1}	0.79	0.78	0.57±0.03 0.7	25 26
H_2 ($D,v'=4$) $E=2800$ cm^{-1}	0.72	0.75		
D_2 ($D,v'=4$) $E=274$ cm^{-1}	0.86	0.86		
H_2 (hypothetical) $E=274$ cm^{-1}		0.82		

Table III some of the results obtained using either the partial cross sections $\sigma_{X\to B}$ and $\sigma_{X\to B'}$, or Eq. (33) with P calculated at the energy of the resonance. It is clear that $\omega=1-P$ reproduces quite well the more accurate results using the calculated values of the partial cross sections. The variation of ω with energy is illustrated by the comparison between $v=3$ and $v=4$ in H_2. The fraction of H(2s) atoms produced diminishes slowly reflecting merely the behavior of P. For D_2 we expect a larger value at the same energy due to a smaller value of P. Since there is no accidental coincidence between vibrational levels of H_2 and D_2 we compare the values of ω for $v=4,R(1)$ of D_2 with a hypothetical H_2 level at the same total energy (see Table III). We notice that indeed $\omega_{D_2}<\omega_{H_2}$.

Some other calculations of ω have been presented in the literature. Komarov and Ostrovsky[17] have studied the problem using covalent and ionic wave functions which cross in the region ~ 15 a.u. However, Borondo *et al.*[42] have found that those states are not diabatic and the radial coupling between them is far from negligible. Borondo *et al.*[17] have calculated ω using *ab initio* adiabatic states and radial coupling. Their calculations were conducted as follows. They assume the B' state to be populated at short distances by predissociation from the D state and the nonadiabatic transitions at larger distances are calculated by solving the appropriate quantum-mechanical close coupling equations. They obtained $\omega=0.70$ practically independent of the energy in the region between 0.1–0.2 eV (800–1600 cm^{-1}). We have found 0.79 at $E=950$ cm^{-1} and 0.72 at $E=2800$ cm^{-1} (see Table III). Thus our ω value is somewhat larger than the one calculated by Borondo *et al.*[17] In addition, our ω changes smoothly but quite significantly with energy. The radial coupling is the same in both calculations, and the adiabatic curves are very similar. However, small changes in the energy difference between the adiabatic curves can affect significantly the branching ratio.

IV. CONCLUSIONS

In this paper we have shown some new effects in the photodissociation of H_2 and D_2 in the 845–820-Å excitation region. The branching ratio $\Omega=\sigma(H(2p))/\sigma(H(2s))$ between the two dissociative channels producing $H(n=2)+H(1s)$ is dramatically changed by the influence of nonadiabatic couplings in the asymptotic region. In particular, we predict an oscillating behavior which is due to quantum interference between two different dissociative paths leading to the same final state. These oscillations could eventually be seen in experiments utilizing the same technique which has been used in the case of predissociation.[25] The total cross section, on the other hand, is not changed significantly from those calculated without including the nonadiabatic couplings and which have been compared favorably with experiments.[13,21]

Recently Nesbitt and Hynes[43] have also considered theoretically the possibility of oscillations in single pass curve crossings. They suggest that they could be proved experimentally via a direct photodissociation process. In their case the oscillations would not come from a quantum interference effect, such as that considered in this work, but from the particular form of the curve crossing and coupling.

In our calculations this would imply that P (the probability for a transition in a single pass) plotted in Fig. 5 is an oscillating function itself. In our case P is smooth and the oscillations come from the quantum interference of two different dissociation paths leading to the same final state of the fragments. They have the same origin as the Stückelberg oscillations in low-energy atom-atom collisions.[44]

Another interesting outcome of our calculations is the prediction of similar oscillations in D_2 but with different amplitudes and periods. The period is essentially governed by phase differences between the vibrational wave functions of the two interacting states in the transition region, while the amplitude depends on the transition probability. Both change with isotopic substitution and therefore provide a direct handle on the nonadiabatic interaction.

Although this interference seems to be particularly dramatic in H_2, it may also occur in other systems. What is only needed is two absorbing continua which are cou-

pled at large internuclear distance. On the other hand, their degeneracy at infinity is not necessary. In particular for the alkali-metal systems, in which nonadiabatic interactions between dissociative states affect the fine-structure branching ratio, constitute good candidates for these interference effects.[45–47] From the theoretical point of view we have shown that the full close-coupling results using the artificial channel method[27] can be very well analyzed in terms of the half collision model which in turn can be deduced from a full collision treatment.

We have also studied the predissociation profiles corresponding to excitation of the $D(^1\Pi_u^+)$. They can be very well accounted for in terms of Fano's perturbation treatment if the influence of discrete as well as the continuous spectrum of the dissociative state is properly included. We confirm the rotational dependence of the various parameters (linewidth, asymmetry, etc.) of the profiles previously predicted in Ref. 33.

Concerning the branching ratios $\sigma(H(2p))/\sigma(H(2p))$ on a predissociation peak, we have found a large discrepancy between calculated and experimental values (see Table III). This was already observed by Borondo *et al.*[9] in their calculations. The reason for it is not fully understood. More experimental data, in particular as a function of energy, is needed in order to settle this problem. An experiment on D_2 would also be very instructive.

ACKNOWLEDGMENTS

The Laboratoire pour l'Utilisation du Rayonnement Electromagnétique is a Laboratóire associé au Centre National de la Recherche Scientifique (CNRS) Commissariat à l'Energie Atomique, and MEN. The Laboratoire de Spectroscopie Hertzienne is associé au CNRS.

[1]W. Kołos and L. Wolniewicz, Can. J. Phys. **53**, 2189 (1975).
[2]W. Kołos and J. Rychlewski, J. Mol. Spectrosc. **62**, 109 (1976).
[3]W. Kołos, J. Mol. Spectrosc. **62**, 429 (1976).
[4]W. Kołos and L. Wolniewicz, J. Mol. Spectorsc. **54**, 303 (1975).
[5]W. Kołos and L. Wolniewicz, J. Chem. Phys. **45**, 509 (1966).
[6]A. L. Ford, E. M. Greenawalt, and J. C. Browne, J. Chem. Phys. **67**, 983 (1977).
[7]W. Kołos and J. Rychlewski, J. Mol. Spectrosc. **88**, 1 (1981).
[8]L. Wolniewicz, J. Chem. Phys. **78**, 6173 (1983).
[9]F. Borondo, J. R. Eguiagaray, and A. Riera, J. Phys. B **15**, 899 (1982).
[10]W. Kołos and L. Wolniewicz, J. Chem. Phys. **51**, 5002 (1969).
[11]L. Wolniewicz, Chem. Phys. Lett. **31**, 248 (1975).
[12]A. L. Ford, J. C. Browne, E. J. Shipsey, and P. Devries, J. Chem. Phys. **63**, 362 (1975).
[13]M. Glass-Maujean, Phys. Rev. A **33**, 342 (1986).
[14]P. J. Julienne, Chem. Phys. Lett. **8**, 27 (1971).
[15]F. Fiquet-Fayard and O. Gallais, Mol. Phys. **20**, 527 (1971).
[16]C. H. Greene and Ch. Jungen, Adv. At. Mol. Phys. **21**, 51 (1985).
[17]I. V. Komarov and V. N. Ostrovksy, J. Phys. B **12**, 2485 (1979).
[18]R. N. Zare, Mol. Photochem. **4**, 1 (1972).
[19](a) R. J. Van Brunt and R. N. Zare, J. Chem. Phys. **48**, 4304 (1968); (b) J. Vigué, P. Grangier, G. Roger, and A. Aspect, J. Phys. (Paris) Lett. **42**, L-531 (1981); (c) J. Vigué, J. A. Beswick, and M. Broyer, J. Phys. (Paris) **44**, 1225 (1983); (d) M. Glass-Maujean and J. A. Beswick (unpublished).
[20]M. Glass-Maujean, J. Breton, and P. M. Guyon, Chem. Phys. Lett. **63**, 591 (1979).
[21]M. Glass-Maujean, P. M. Guyon, and J. Breton, Phys. Rev. A **33**, 346 (1986).
[22]M. Glass-Maujean, J. Breton, and P. M. Guyon, J. Chem. Phys. **83**, 1468 (1985).
[23]M. Glass-Maujean, J. Breton, B. Thièblemont, and K. Ito, Phys. Rev. A **32**, 947 (1985).
[24]M. Rothschild, H. Egger, R. J. Hawkins, H. Pummer, and C. K. Rhodes, Chem. Phys. Lett. **72**, 404 (1980).
[25]J. E. Mentall and P. M. Guyon, J. Chem. Phys. **67**, 3845 (1977).
[26]J. E. Mentall and E. P. Gentieu, J. Chem. Phys. **52**, 5641 (1970).
[27]M. Shapiro, J. Chem. Phys. **56**, 2582 (1972).
[28]F. T. Smith, Phys. Rev. **179**, 111 (1969).
[29]K. C. Kulander and J. C. Light, J. Chem. Phys. **73**, 4337 (1980); R. W. Heather and J. C. Light, *ibid.* **78**, 5513 (1983); **79**, 147 (1983).
[30]R. Schinke and V. Engel, J. Chem. Phys. **83**, 5068 (1985).
[31]D. C. Clary, J. Chem. Phys. **84**, 4288 (1986).
[32]M. Shapiro and R. Bersohn, Annu. Rev. Phys. Chem. **33**, 409 (1982).
[33]P. H. Guyon, J. Breton, and M. Glass-Maujean, Chem. Phys. Lett. **68**, 314 (1979).
[34]B. R. Johnson and D. Secrest, J. Chem. Phys. **48**, 4682 (1968).
[35]J. H. Ahlberg, E. N. Nilson, and J. L. Walsh, *The Series of Splines and Their Applications* (Academic, New York, 1967); J. R. Rice, *The Approximations of Functions* (Addison-Wesley, Reading, Mass., 1969), Vol. 2.
[36]N. F. Mott and H. S. W. Massey, *The Theory of Atomic Collisions* (Clarendon, Oxford, 1965), pp. 346–354; M. S. Child, *Molecular Collision Theory* (Academic, New York, 1974), pp. 161–179; H. Nakamura, J. Phys. Chem. **88**, 4812 (1984).
[37]J. R. Taylor, *Scattering Theory* (Wiley, New York, 1972).
[38]M. Glass-Maujean, J. Chem. Phys. **85**, 4830 (1986).
[39]J. J. Hopfield, Nature **125**, 927 (1930).
[40]H. Beutler, A. Deubner, and H. O. Jünger, Z. Phys. **98**, 181 (1935).
[41]U. Fano, Phys. Rev. **124**, 1866 (1961).
[42]F. Borondo, A. Macias, and A. Riera, J. Chem. Phys. **74**, 6126 (1981).
[43]D. J. Nesbitt and J. T. Hynes, J. Chem. Phys. **84**, 1554 (1986); see also, W. H. Miller, J. Chem. Phys. **85**, 3703 (1986).
[44]See, for example, M. S. Child, in *Atomic and Molecular Collision Theory,* Vol. 71 of NATO ASI, Series B, Physics, edited by F. A. Gianturo (Plenum, New York, 1982).
[45]E. A. Gordeev, E. E. Nikitin, and A. I. Shushin, Mol. Phys. **33**, 1611 (1977).
[46]V. B. Grushevskii, S. M. Papernov, and M. L. Yanson, Opt. Spectrosk. **44**, 809 (1978) [Opt. Spectrosc. (USSR) **44**, 475 (1978)].
[47]S. J. Singer, K. F. Freed, and Y. B. Band, Chem. Phys. Lett. **110**, 588 (1984); Adv. Chem. Phys. **61**, 1 (1985).